**Surface Investigation and Morphological Analysis of Structurally Disordered MgCl2 and MgCl2/TiCl4 Ziegler-Natta Catalysts**

# UNIVERSITÀ DEGLI STUDI DI TORINO

# Surface Investigation And Morphological Analysis Of Structurally Disordered $MgCl_2$ And $MgCl_2/TiCl_4$ Ziegler-Natta Catalysts

Maddalena D'Amore,[1] K.S. Thushara,[1] Alessandro Piovano,[1] Mauro Causà,[2] Silvia Bordiga,[1] Elena Groppo[1,*]

[1] Department of Chemistry, INSTM and NIS Centre, University of Torino, Via Quarello 15, 10135 Torino, Italy.

[2] Department of Chemical, Materials and Production Engineering, University of Naples Federico II, Piazzale Tecchio, 80126 Napoli, Italy.

**ABSTRACT:** Activated $MgCl_2$ nano-crystals were prepared by controlled de-alcoholation of the $MgCl_2 \cdot 6CH_3OH$ adduct, mimicking the routinely adopted methods to synthetize industrial heterogeneous Ziegler-Natta catalysts. The effect of the alcohol in driving the morphology of $MgCl_2$ crystals, i.e. the type and extension of the exposed surfaces, was investigated by integrating a detailed structural, morphological and surface characterization with a state-of-the-art computational modeling. FT-IR spectroscopy of CO adsorbed at 100 K emerged as a feasible, simple and powerful method to characterize the surface of structurally disordered $MgCl_2$ and $MgCl_2$-based Ziegler-Natta catalysts. Our computational morphological analysis revealed that the (012), (015) and (110) surfaces are highly stabilized by methanol as an electron donor, especially at the temperature typically adopted in the preparation of the pre-catalysts. FT-IR spectroscopy of adsorbed CO allows to distinguish these surfaces from the other penta-coordinated ones, and provides a clear experimental evidence that $TiCl_4$ binds to the (110) and (015) surfaces. The (015) surface was never considered in the past, and is characterized by an unusual flexibility in presence of adsorbates, which detach the Mg cations from the Cl underneath, leaving a coordination vacancy available for the binding of asymmetric titanium sites. Since the recent literature identified a tetra-coordinated Mg as a site of election for the deposition of the Ti species relevant in olefin polymerization, the presence of two eligible Mg sites for Ziegler-Natta catalysis is highly interesting.

**KEYWORDS**: Ziegler-Natta catalysts; magnesium chloride; titanium chloride; in situ FT-IR spectroscopy; DFT-D calculations

## 1. INTRODUCTION

The discovery in the late 1960s of $MgCl_2$ as a support material for the Ziegler-Natta catalysts revolutionized the scenario of the polyolefin technology. Today more than 80 million tonns/year of polyolefins are produced using the $MgCl_2$-supported Ziegler-Natta catalysts.[1,2] Even though the catalysts composition underwent successive modifications by the introduction of new components (i.e. electron donors), which are fundamental to achieve stereo-selectivity in α-olefin polymerization, the main constituents are still the same since several decades: $TiCl_4$ (as precursor of the active sites), $MgCl_2$ (as support), and an aluminium alkyl (or aluminium alkyl chloride, as a co-catalyst). Despite more than sixty years of success in the industrial production of polyolefins and many decades of academic research, the basic understanding of these systems is still poor.

It is known that structurally disordered $MgCl_2$ is the active support interacting with $TiCl_4$. Disordered $MgCl_2$ is usually synthesized in the presence of $TiCl_4$ following either mechanical or chemical routes. In mechanical methods, $MgCl_2$ and $TiCl_4$ are ball milled with or without the solvent to generate the active catalyst. In chemical routes, highly crystalline $MgCl_2$ (α form) is interacted with Lewis bases (mainly alcohols), then dealcoholated or reacted with $TiCl_4$ to form disordered $MgCl_2$ (δ form).[3-7] The pioneering works of Corradini and co-workers suggested models for $MgCl_2$ where, besides the (100) basal planes (which are fully covered by chlorine and hence of no interest for catalysis), the two coordinatively unsaturated (104) and (110) (and equivalent) surfaces were the most favourite ones.[8,9] Recent theoretical calculations on $MgCl_2$ bulk and surface structure by means of periodic Density Functional Theory methods including dispersion (DFT-D) confirm the old scenario:[10] well-formed $MgCl_2$ crystals in the absence of adsorbates predominantly feature the (104) surfaces, while the (110) faces were found to be too high in energy and hence are expected to be formed only for crystals grown under kinetic control and unable to reconstruct. However, the situation drastically changes in the presence of adsorbates (including electron donors). Recent DFT-D studies[11-13] demonstrated that $MgCl_2$ crystals mainly expose the (110) surfaces when they are formed in the presence of Lewis bases (especially small molecules such as methanol, ethanol, and dimethyl ether) or in presence of silanes adopted as external donors.

The distribution and extension of the $MgCl_2$ surfaces influence the structure and properties of the supported $TiCl_x$ sites in the $MgCl_2/TiCl_4$ pre-catalyst and ultimately have important effects on the properties of the reduced active Ti sites. Following the seminal Corradini model, $TiCl_4$ would epitactically adsorb in the monomeric form on the (110) surface giving rise to a non-stereospecific site; whereas $Ti_2Cl_8$ dimers would be formed on the (104) surface, with stereospecific properties. Although this model is still widely

accepted in a large scientific community, it was recently questioned by modern quantum mechanical calculations. The emerging picture is very different from the original one and suggests that interaction of $TiCl_4$ and $Ti_2Cl_8$ species with $MgCl_2$ surfaces is very weak. The only model which may be possible is that of monomeric $TiCl_4$ on $MgCl_2$ (110) surface, but weak binding is predicted also in this case.[14]

Opposite to the huge number of theoretical works, a very limited number of experimental data are available in literature to confirm the computational predictions. The presence of multi components interacting with each other and their sensitivity to moisture are the main difficulties encountered in the attempt to investigate these systems from an experimental point of view.[15] Surface science methods are necessary to characterize the exposed sites at the surface of the disordered $MgCl_2$ and of the corresponding $MgCl_2/TiCl_4$ catalysts. In this respect, it is worth mentioning the pioneering works of Somorjai and his group,[16-21] later on followed by Freund and co-workers,[22-24] who investigated "surface science" models of Ziegler-Natta catalysts. Among the main findings, it is important to recall here the observation that $TiCl_4$ does not bind to the $MgCl_2$ surface, unless structural defects are created in $MgCl_2$, a finding that confirms the weak binding between $TiCl_4$ and $MgCl_2$. However, the synthesis conditions for the pre-catalysts are far from those used industrially; hence, the relevance of these experimental results for industrial catalysts may be questioned. More recently, Thune and colleagues developed a method to realize planar models of $MgCl_2/LB/TiCl_4$ systems (where LB = Lewis basis), starting from the spin-coating of a $MgCl_2{\cdot}ROH$ solution, followed by the gradual replacement of the alcohol with $TiCl_4$.[25-28] The method, which mimics some industrial procedures for Ziegler-Natta catalysts preparation, allowed the application of "surface science" techniques and microscopies to investigate the catalyst surface. Nevertheless, the obtained experimental results are difficult to be compared with theoretical calculations. As a matter of fact, the pre-catalyst is obtained in situ in presence of an excess of Lewis basis and $TiCl_4$, whereas calculations are usually performed on well-defined $MgCl_2$ surfaces by progressively adding $TiCl_4$ and/or Lewis basis molecules one after the other.

In this work we propose an innovative approach, which integrates state-of-the-art computational modelling with an experimental strategy having simultaneously a synthetic and a characterization goal. An activated $MgCl_2$ support is prepared in situ by controlled de-alcoholation of $MgCl_2{\cdot}6MeOH$ adduct (MeOH = methanol), mimicking the routinely adopted methods to synthetize industrial heterogeneous Ziegler-Natta catalysts.[29,30] The effect of methanol in driving the morphology of $MgCl_2$ crystals, i.e. the type and extension of the exposed surfaces, is investigated. De-alcholated $MgCl_2$ is initially characterized in terms of structure and morphology, by means of X-ray Powder Diffraction (XRPD), $N_2$ physisorption measurements and High-Resolution Transmission Electron Microscopy (HR-TEM). These experimental data are compared with the results of a systematic computational work conducted with a DFT-D approach and aimed at evaluate the relative stability of the $MgCl_2$ surfaces both in the absence and in the presence of methanol molecules. In turns, the surface energy and the relative growth rate for the various surfaces determine the equilibrium morphology of a $MgCl_2$ crystal, according to the Gibbs-Wulff theory which predicts that the equilibrium crystal shape should possess a minimal total surface energy for a given volume.[31,32] A surface with a high surface free energy has a large growth rate, and this fast growing surface will not be expressed in the equilibrium morphology of the resulting crystal. Therefore, only surfaces with low surfaces energies and hence slow growth will be expressed. It is well known that at 0 K the surface free energy is a close approximation of the surface energy as calculated by static lattice simulations, being the entropy term small. Hence, the equilibrium morphology of a crystal is usually determined by considering the surface energy only. With the only exception of ethanol absorption on "classical" (104) and (110) surfaces,[11] up to now the papers describing adsorption of donor molecules on $MgCl_2$ surfaces reported only estimates of enthalpy,[11-13] since calculation of entropy contributions for surface-adsorbed species is a tedious and time consuming process. However, chemical processes are driven by free energy, and any calculation intended to predict chemical behaviours should produce free energy values. For this reason we underwent an absolutely novel systematic vibrational analysis at the periodic level to predict the $MgCl_2$ crystal shape in presence of methanol taking into account also the entropic term.

In the second part of the work we investigate the surface properties of the de-alcholated $MgCl_2$, and of the corresponding pre-catalyst obtained upon its titanation in presence of $TiCl_4$ vapours, by means of FT-IR spectroscopy of CO adsorbed at 100 K, which allows to characterize the number and type of exposed surfaces. Assignment of the experimental $\tilde{\nu}$(CO) data is done by comparison with theoretically computed $\tilde{\nu}$(CO) values for CO adsorbed on the $MgCl_2$ model emerging from the morphological analysis. The good agreement between experiments and theory proves that FT-IR spectroscopy of adsorbed CO is a valuable method to investigate the surface of $MgCl_2$ nano-crystals, opening interesting perspectives in the characterization of $MgCl_2$-supported Ziegler-Natta catalysts.

## 2. EXPERIMENTAL

All the syntheses and reactions were performed under dry nitrogen atmosphere using standard Schlenk techniques. Dry $MgCl_2$, titanium tetrachloride, anhydrous methanol, and anhydrous solvents (n-hexane and toluene), all from Sigma Aldrich, were used as received.

**2.1 Synthesis of the active $MgCl_2$ phase ($MgCl_{2\text{-act}}$).** The $MgCl_2{\cdot}6MeOH$ adduct was synthesized using a well-established azeotropic distillation method, as reported in Ref. [33,34]. The active $MgCl_2$ phase was obtained from the $MgCl_2{\cdot}6MeOH$ adduct, through a controlled de-alcoholation in dynamic vacuum at 473 K for prolonged time. A general procedure is as follows. The $MgCl_2{\cdot}6MeOH$ adduct is heated under dynamic vacuum ($5\ 10^{-4}$ mbar) up to 473 K at a heating ramp of 2 K/min, left at that temperature overnight, and finally cooled at room temperature. The de-alcoholation step must be performed directly into the cell used for the characterization, in order to avoid poisoning.

**2.2 Synthesis of the pre-catalyst ($MgCl_{2\text{-act}}/TiCl_4$).** The $MgCl_{2\text{-act}}/TiCl_4$ pre-catalyst was prepared by titanating the $MgCl_{2\text{-act}}$ support in the presence of $TiCl_4$ vapours at 353 K. $TiCl_4$ in excess was removed by degassing at the same temperature. The procedure was standardized in order to obtain a final titanium loading close to 1.0 wt% with respect to $MgCl_2$ (as determined by ICP analysis), a value which is

comparable to that characteristic of industrial $MgCl_2/TiCl_4$ pre-catalysts.

**2.3. Characterization techniques.** *X-ray Powder Diffraction (XRPD).* XRPD patterns were collected with a PW3050/60 X'Pert PRO MPD diffractometer from PANalytical working in Debye-Scherrer geometry, using as source the high power ceramic tube PW3373/10 LFF with a Cu anode, equipped with Ni filter to attenuate Kβ and focused by X-ray mirror PW3152/63. Scattered photons were collected by a RTMS (Real Time Multiple Strip) X'celerator detector. All the samples were measured as powders inside a 1 mm boron-silicate capillary, filled in the glove box and sealed in inert atmosphere.

*$N_2$-physisorption measurements.* Nitrogen adsorption measurements at 77 K were performed on a ASAP 2020 instrument. The surface area and pore-size distribution of $MgCl_{2\text{-act}}$ was determined by Brunauer–Emmett–Teller (BET) method.

*High Resolution Transmission Electron Microscopy (HR-TEM).* HR-TEM measurements were performed on a JEOL 2000 EX instrument equipped with a top entry stage and operating at 200 kV. The $MgCl_2 \cdot 6MeOH$ adduct was deposited directly from a methanol solution on a carbon – covered copper grid and kept under inert atmosphere during all the steps of manipulation. De-alcoholation and formation of activated $MgCl_2$ is observed directly under the electron beam.

*FT-IR spectroscopy.* FT-IR spectra were acquired in transmission mode on a Bruker Vertex70 spectrophotometer equipped with a MCT detector, at a resolution of 2 $cm^{-1}$. The samples were measured in the form of self-supporting pellets inside a quartz cell equipped with KBr windows, allowing to perform measurements in the 293 - 100 K temperature range. The standard procedure was as follows. A thin self-supporting pellet of the $MgCl_2 \cdot 6MeOH$ adducts is prepared in the glove box and placed inside the measurement cell, which allows to perform thermal treatments in high vacuum or in presence of gases. De-alcoholation of $MgCl_2 \cdot 6MeOH$ to obtain $MgCl_{2\text{-act}}$ is performed directly in the measurement cell. Any attempt to obtain $MgCl_{2\text{-act}}$ ex-situ and to transfer it into the FT-IR cell failed: even by using a perfectly clean glove-box (both $O_2$ and $H_2O$ below 0.5 ppm), the $MgCl_{2\text{-act}}$ was inevitably poisoned by residual moisture. The reaction cell with self-supporting pellet of $MgCl_{2\text{-act}}$ is then connected to a vacuum line which allows gas dosage. CO is dosed at room temperature (equilibrium pressure $P_{CO}$ = 50 mbar), and the temperature is gradually decreased down to 100 K. FT-IR spectra are collected at 100 K at different degrees of CO coverage ($\theta$), starting from CO full coverage ($\theta_{max}$) and gradually decreasing the equilibrium pressure through controlled expansions.

## 3. COMPUTATIONAL METHODS AND MODELS

**3.1 Geometry optimization.** All *ab initio* calculations were performed using the CRYSTAL14 periodic code, which employs a Gaussian type basis set.[35] The simulations were done within the framework of Density Functional Approximation (DFT). The hybrid Becke, three parameters, Lee-Yang-Parr (B3LYP) functional was adopted.[36] A general drawback of all common GGA functionals, including hybrids, is that they cannot describe long-range electron correlations that are responsible for van der Waals (dispersive) forces. Since dispersion plays a key role in many chemical systems and, in particular, it has a role in determining the orientation of donor molecules on surfaces, it was necessary to apply a correction to the energy obtained with the standard density functional methods. When dispersion is included in the system, the total computed energy is given by Equation 1.1.

$$E_{DFT-D} = E_{DFT} + E_{disp} \quad (1.1)$$

where $E_{disp}$ is the empirical dispersion correction originally proposed by Grimme[37] and referred to as the D2 correction (Equation 1.2).

$$E_{disp} = S_6 \sum_g \sum_{ij} f\left(R_{ij,g}\right) \frac{C_6^{ij}}{R_{ij,g}^6} \quad (1.2)$$

In Equation 1.2 the summation is over all atom pairs *i, j* and lattice vectors **g** which define the cells of the $j^{th}$ atom, with the exclusion of the $i = j$ contribution for **g** = 0; $C_6^{ij}$ is the dispersion coefficient for the $ij^{th}$ pair of atoms; *f* is a damping function used to avoid near-singularities for small inter-atomic distances $R_{ij,g}$; $S_6$ is a scaling factor that depends on the adopted DFT method (for B3LYP $S_6$= 1.0). For the specific case of B3LYP calculations, the modification proposed by Civalleri and co-workers[38] to a Grimme's standard set of parameters has been adopted. The corrections (when activated during a geometry optimization), were added to the energy and its gradient to determine the final geometry. The inclusion of dispersive forces during the optimization highlights their role in determining the most stable geometry of adsorption.

Split valence triple-ζ basis sets plus polarization (TZVP) functions have been applied to describe all the elements (Mg, Ti and Cl atoms).[14] An Ahlrichs VTZ[39] plus polarization quality has been adopted for the adsorbed methanol molecules, whereas the coefficients of the polarization Gaussian functions ($\alpha_{poi}$) were optimized in preliminary studies performed on similar systems employing alcohols[11] thus enabling more accurate calculations of adsorption energy and vibrational frequencies. The choice was aimed at reducing the Basis Set Superposition Error (BSSE), that may become quite large in particular when the dispersion correction is included during the optimization process, i.e. when the molecule and the surface become closer. It was demonstrated that the BSSEs amount at about 12% of computed total adsorption energy, indicating that the 'customized' Ahlrichs basis sets adopted are adequate.

The Gauss-Legendre quadrature and Lebedev schemes were used to generate angular and radial points of a pruned grid consisting of 75 radial points and maximum number of 974 angular points over which electron density and its gradient were integrated.[40] Values of the tolerance that control the Coulomb and exchange series in periodical systems were set to 7 7 7 7 18. All the bielectronic integrals, Coloumb and exchange, were evaluated exactly.

For all B3LYP-D calculations, 10 K points have been adopted. Internal coordinates and cell parameters have been optimized using the analytical gradient method to optimize the atomic positions.

**3.2 Calculation of methanol adsorption energy.** In order to calculate the relative stability of $MgCl_2$ surfaces in presence of methanol the following systematic approach was adopted. At first, the interaction energy, $\Delta E_{ads}$, per unit cell per adsorbate methanol molecule was calculated for all the stable surfaces of $MgCl_2$. For a bounded system $\Delta E_{ads}$ is a negative quantity, defined according to the Equation 1.3:

$$\Delta E_{ads} = \frac{(E_{adduct} - E_{slab} - x E_D)}{x} \quad (1.3)$$

where $E_{adduct}$ is the electronic energy of a relaxed surface slab in interaction with the adsorbate molecule; $E_{slab}$ is the energy of a relaxed slab alone as obtained by cut from a fully optimised bulk $MgCl_2$ (α-form); $E_D$ is the molecular energy of the free fully optimized adsorbate molecule, and $x$ is the number of adsorbed molecules per unit cell. All $\Delta E_{ads}$ values are given per coordinated mole of donor (regardless of its coordination mode), using fully relaxed unit cells for bare and covered crystals.

Successively, a vibrational analysis was carried out to calculate $\Delta S_{ads}$ both at standard conditions (P = 1 bar, T = 298 K) and in conditions close to those involved in the formation of $MgCl_2$ crystals from alcohol adducts (P = 1 bar, T = 373 K). The Gibbs free energy of adsorption, $\Delta G_{ads}$, was calculated as in Equation 1.3 with $G$ instead of $E$.[41] The Gibbs free energy of methanol-covered surfaces ($G_{s\text{-}MeOH}$) was successively calculated by adding $\Delta G_{ads}$ to the formation energy of each naked surface ($G_{s\text{-}MeOH} = G_s + \Delta G_{ads}$) and expressed in J/m$^2$. Differently from most available periodic codes which are based on the plane-wave basis sets in combination with pseudo-potentials, the CRYSTAL14 code employs Gaussian type local basis sets and therefore allowed easy implementation of hybrid functionals such as B3LYP, which is important in view of the proven reliability of these functionals in computing vibrational properties.[42-44] The vibrational analysis used is similar to the computational scheme of many molecular codes, using analytical gradients of energy with respect to nuclear positions and numeric differentiation to obtain the hessian at the central point of the first Brillouin zone (Γ point, point $k = 0$ in BZ).

To estimate zero point energy, thermal and entropy contribution in evaluation of Gibbs free energy, vibrational frequencies at the Γ point were computed in the harmonic approximation by diagonalizing the mass-weighted Hessian matrix. Second derivatives are calculated numerically by using analytical first derivatives and finite displacements of the atomic positions. The results obtained with the default in CRYSTAL14 code of one difference quotient formula, where one displacement for each atom along each cartesian direction has been considered, were compared with those obtained with two central-difference formula,[35] i.e. two displacements of each atom along each Cartesian direction. In the two cases the contribution to Gibbs free energy was almost the same.

A degree of coverage θ (defined as θ = areal density of adsorbates/areal density of surface atoms) equal to 1 is reached when every exposed Mg atoms are coordinated by one donor molecule. When building models of methanol adsorbed on $MgCl_2$ surfaces, $\theta_{MeOH}$ was assumed equal to 1 for surfaces exposing penta-coordinated $Mg^{2+}$ sites ($Mg_{5c}^{2+}$) like the (104), whereas also a value $\theta_{MeOH}$ =2 was considered for surfaces exposing $Mg_{4c}^{2+}$ sites, like the (110) surface.

**3.3 Prediction of $MgCl_2$ crystal shape.** The following procedure was adopted to obtain a reasonable prediction of $MgCl_2$ crystals' shape by CRYSTAL code.[45] At first, an analysis of the α-$MgCl_2$ planes was performed to locate the most stable surfaces of the crystals. According to Bravais' law, the faces that appear on a crystal will be parallel to the lattice planes with the larger distance between planes. In fact the surface free energy is inversely proportional to the directional density and thus proportional to $d_{hkl}$. Similarly, morphological simulation by Bravais (1866), Friedel (1907) and Donnay and Harker (1937) ended in the BFDH law: due to space group symmetry, the most important crystallographic forms will have the greatest inter-planar spacing. Crystallographic planes have been indexed and printed, grouped in families of symmetry-related planes. The {hkl} planes that have the interplanar distance in the range $\left(f\, d_{hkl}, d_{hkl}^{max}\right)$ have been analysed, where $d_{hkl}^{max}$ is the maximum interplanar distance for a given plane {hkl} and f is a factor between 0 and 1.

The form of small crystals can be discussed in terms of thermodynamics of surfaces. At equilibrium at a certain temperature T, a small crystal has a specific shape that corresponds to a crystal with exposed *hkl* faces such that the integration on the entire surface area A, $\int \gamma(hkl)A(hkl)$, is minimal, i.e. the total surface free energy according to the Wulff-Gibbs theorem is a minimum. For each corresponding slab the most stable family of planes were considered and Gibbs free energies evaluated before and after the donor adsorption.

**3.4 CO adsorption.** For most of the surfaces the adsorption of CO has been modelled adopting the same level of calculation described above and also an Alrichs QTZV plus polarization[32] (QTZVP2) quality basis set. The coefficients of the polarization Gaussian functions ($\alpha_{pol}$) were optimized in a previous study on adsorbed CO,[46] and vibrational frequencies at the Γ point were computed as described in section 3.2. Infrared intensities are evaluated through Berry phase approach,[47] consisting in evaluating the atomic Born tensors from the polarizations generated by small atomic displacements (the same as for the second energy derivative).

## 4. RESULTS AND DISCUSSION

**4.1 Structure, texture and morphology of $MgCl_{2\text{-}act}$ at the nanoscale.** Activated $MgCl_2$ was obtained by controlled de-alcoholation of the $MgCl_2$·6MeOH adduct in dynamic vacuum upon increasing the temperature up to 473 K. According to thermo-gravimetric analysis (Figure S1) all the methanol molecules are stoichiometrically removed at the end of the process. Nevertheless, the FT-IR spectrum of the so obtained $MgCl_{2\text{-}act}$ sample (Figure S2) still shows a few weak absorption bands in the Mid-IR region which are reminiscence of the alcohol species present in the starting adducts. In addition, an absorption band around 720 cm$^{-1}$ is observed, which is assigned to ν(Mg-O) vibrational modes. These remaining alcohol molecules (or their by-products) likely occupy defect sites (corners, edges) at the $MgCl_2$ surface.

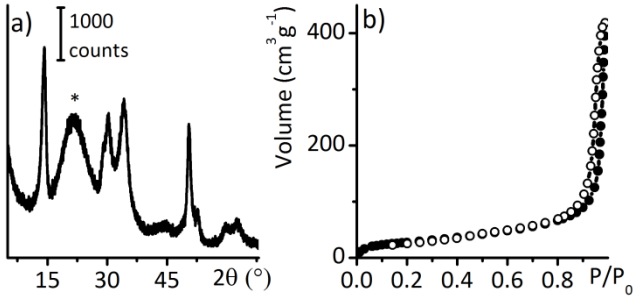


Figure 1. Part a) XRPD pattern of $MgCl_{2\text{-}act}$. The broad peak labeled with asterisk is associated to the glass capillary. Part b) $N_2$ physisorption isotherm collected at 77 K for $MgCl_{2\text{-}act}$. Adsorption

and desorption data are shown with filled and empty symbols, respectively.

Indeed, the XRPD pattern of $MgCl_{2\text{-act}}$ (Figure 1a) is characteristics of a layered δ-$MgCl_2$ phase, with extensive structural disorder, in agreement with literature findings.[48-51] The diffraction peak around 2θ = 15° (d = 5.90 Å) corresponds to the (001) basal plane and its broadness is related to the average dimensions of the crystalline domains along the c-axis, i.e. to the stacking degree of the (001) planes. The position and shape of the diffraction peak around 2θ = 50°, corresponding to the (110) plane, depend principally on the dimensions of the $MgCl_2$ domains in the ab plane. Finally, broad asymmetric halos are observed in the 2θ = 30-37° and 2θ = 55-65° ranges.

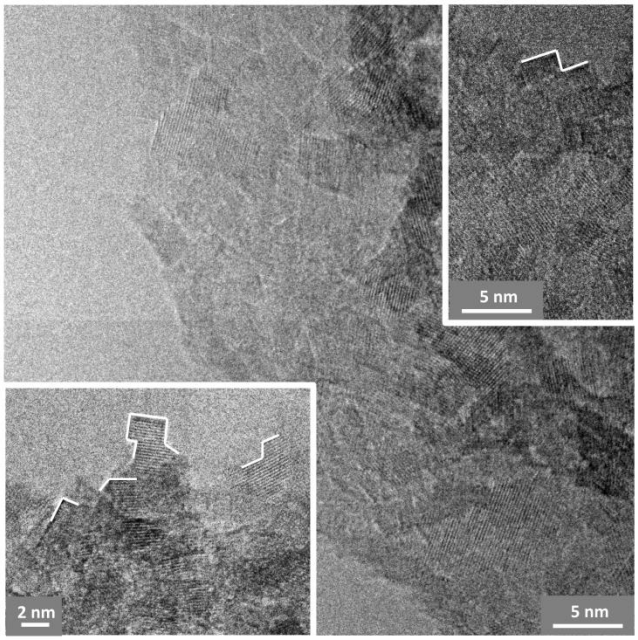


Figure 2. Representative HR-TEM pictures of $MgCl_{2\text{-act}}$. White segments are a guide to highlight the edges of the nano-crystals. Both 90° and 120° edge angles can be found.

These halos are usually observed in the XRD pattern of the active δ-form of $MgCl_2$ and have been reported to be very sensitive to the degree of disorder along the c-axis.[48-51] According to Chang et al.,[52] several planes contribute to the 30-37° region, among which the (104) and the (015) are the principal ones. It is worth noticing that a disordered array of $MgCl_2$ units characterized by a chain-like structure and forming a three-dimensional network may present similar Bragg reflections, despite the high degree of structural disorder.[48,49]

The surface area and the porosity of $MgCl_{2\text{-act}}$ was evaluated by $N_2$ volumetric measurements at 77 K. The adsorption isotherm (Figure 1b) is of Type IV, and is characterized by a pronounced hysteresis loop, which reveals the presence of mesopores (probably inter-particles). The specific surface area, evaluated by means of the BET model, is as high as 100 $m^2/g$, and the pore volume is of 0.39 $cm^3/g$. This value is comparable with the specific surface area reported for other $MgCl_2$ samples obtained by chemical or mechanical methods, and also with the values reported for titanated $MgCl_2/TiCl_4$ pre-catalysts,[53,54] confirming that our synthetic approach leads to an activated $MgCl_2$ of potential catalytic relevance.

A few representative HR-TEM images of $MgCl_{2\text{-act}}$ are shown in Figure 2. Although several research groups have reported electron microscopic investigations of polyolefins made on Ziegler-Natta catalysts,[55,56] to the best of our knowledge very few works report electron microscopies directly on $MgCl_2$ samples.[28,57] Indeed, manipulation of the samples without exposing to air is extremely challenging, and in addition they are also very sensitive to radiation damage under the electron beam. Only Mori et al.[57] reported a few HR-TEM images of crystalline $MgCl_2$. Hence, those reported in Figure 2 are the first HR-TEM pictures of an active $MgCl_2$ sample obtained via chemical methods. The $MgCl_{2\text{-act}}$ sample is characterized by the presence of nano-crystalline regions, displaying the characteristic lattice fringes due to the (001) basal plane (d = 5.90 Å), as determined by electron diffraction. The crystalline regions are small, both in the lateral dimensions of the $MgCl_2$ platelets as well as in the degree of stacking along the (001) directions, in agreement with the observations of Andoni et al.[28] on well-defined $MgCl_2$ crystallites obtained from $MgCl_2$·6EtOH adducts large enough to be characterized by SEM. At the borders, well-defined crystals of nanometric size were observed, most of them characterized by lattice fringes due to the (001) planes. Most of the nano-crystals terminate with flat surfaces, in some cases parallel to the lattice fringes and in some others perpendicular to them. Some of them are rectangular in shape (i.e. with 90° edge angles), an evidence that has been previously interpreted as indicative of the co-presence of both the (110) and (104) crystallite surfaces,[28] but also 120° edge angles are observed. The nanometric size of the crystals makes difficult the identification of electron diffraction spots.

**4.2 Predicted $MgCl_2$ crystal shape in presence of methanol.** Parallel to the experimental characterization of $MgCl_{2\text{-act}}$, we carried out periodic DFT-D calculations aimed at elucidating the structures and relative stabilities of several $MgCl_2$ crystal surfaces, for both naked $MgCl_2$ and methanol-covered $MgCl_2$. It is worth noticing that a valuable investigation of the bulk and surface structure of the ordered α and β phases of $MgCl_2$ by means of periodic DFT-D methods was previously reported by Credendino et al.,[58] following the seminal work of Busico et al.[10] still performed without considering dispersion contributions. However, in both works the entropic term was neglected. The results of our analysis, containing the first systematic analysis of 'planes' by means of the CRYSTAL code, are summarized in Table 1, where the exposed surfaces have been ordered following the decrease of $d_{hkl}$. For each surface, the surface energy ($E_s$) and the Gibbs free energy ($G_s$) are reported, both of them normalized to the surface area. Representations of the main surfaces after relaxation are shown in Figure 3.

**Table 1. Most stable surfaces for naked $MgCl_2$, ordered as a function of $d_{hkl}$ in Å, coordination number of the exposed Mg cations, and predicted stability in terms of both surface energy ($E_s$), and Gibbs free energy ($G_s$) evaluated at 298 K and 373 K and expressed in J/$m^2$.**

| **Naked $MgCl_2$** | | | | | |
|---|---|---|---|---|---|
| surface | $d_{hkl}$ (Å) | **Mg C.N.** | **$E_s$ (J/$m^2$)** | **$G_s$ 298K** | **$G_s$ 373K** |

| | | | | $(J/m^2)$ | $(J/m^2)$ |
|---|---|---|---|---|---|
| (001) | 5.739 | 6 | 0.0733 | 0.0498 | 0.0429 |
| (101) | 3.148 | 5 | 0.284 | 0.605 | 0.676 |
| (012) | 3.001 | 5 | 0.311 | 0.558 | 0.612 |
| (104) | 2.569 | 5 | 0.208 | 0.682 | 0.789 |
| (015) | 2.345 | 5 | 0.257 | 0.456 | 0.502 |
| (107) | 1.951 | 5 | 0.230 | 0.387 | 0.442 |
| (110) | 1.849 | 4 | 0.324 | 0.911 | 1.036 |

In agreement with earlier works,[10,58] the (001) basal surface, where all Mg cations are hexa-coordinated as in the bulk crystal, is the most stable one. The surfaces exposing penta-coordinated Mg cations, (104), (101), (012), and (107) are slightly less stable. Calculated $E_s$ values are in well agreement with those reported previously.[58] Curiously, an inversion in the relative stability of the penta-coordinated surfaces is observed

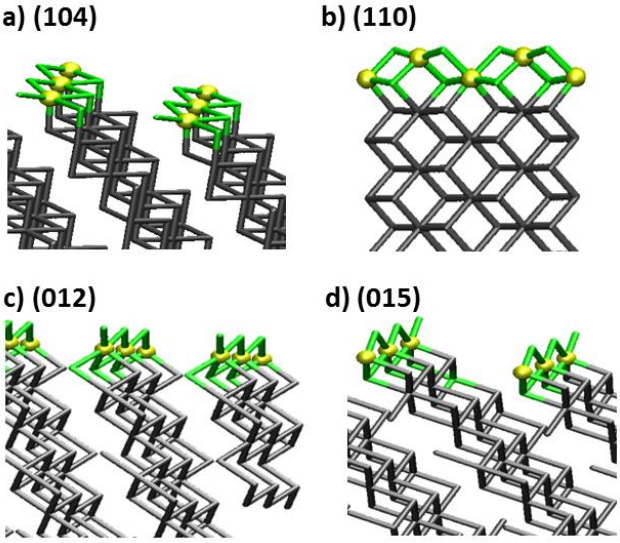


Figure 3. Representation of the main $MgCl_2$ surfaces after relaxation. Bulk $MgCl_2$ is represented in grey. Surface chlorine and magnesium atoms are shown in green and yellow, respectively.

when looking at the $G_s$ values, being now the (104) surface the less favoured one. However, the $G_s$ values of the penta-coordinated surfaces are quite similar. Indeed, these surfaces are actually identical when looking at a single layer of $MgCl_2$, while they differ only when considering the adjacent layers (see e.g. the (104) and the (012) surfaces, Figure 3a and c).[58] The (110) surface (Figure 3b) is by far less stable, even more when the entropic term is considered.[59] The (015) surface (Figure 3d) is more stable and competitive with the other penta-coordinated ones. Interestingly, this surface was never considered in previous computational studies, and it has been identified as possible surface only thanks to the new tool implemented in CRYSTAL14 code. It is worth noticing that the tetra-coordinated (015) slab as cut from the bulk and optimized by maintaining a high level of symmetry (Figure S3) is not the most stable minimum. A new, more stable structure can be found by reducing the symmetry to the inversion centre only, that guarantees the equivalence of the two sides of the slab. In this rearranged surface the Mg cations are virtually penta-coordinated, but display a distorted local geometry.

The relative stability of the $MgCl_2$ surfaces drastically changes when they are covered by methanol, in agreement with earlier works performed on $MgCl_2$ clusters of different size and morphology.[11-13] Table 2 reports the predicted adsorption energies for methanol on different $MgCl_2$ surfaces ($\Delta E_{ads}$ and $\Delta G_{ads}$), and the stability of these surfaces in presence of methanol ($G_{s\text{-}MeOH}$). For all the surfaces, calculations were performed considering a methanol coverage of $\theta_{MeOH} = 1$, and for the (110) and (015) surfaces also $\theta_{MeOH} = 2$ was considered, although a second methanol molecule is stable only on the (110) surface. Calculations were first performed at 298 K, and successively repeated at a temperature of 373 K. Indeed, the de-alcoholation of the $MgCl_2 \cdot 6MeOH$ adduct and the formation of the activated $MgCl_2$ nano-crystals occurs in the 298 – 473 K temperature range. Also the typical processes for the preparation of $MgCl_2$ supports with improved controlled morphology starting from $MgCl_2$ alcoholate adducts are conducted around 373 K. In the presence of methanol at 298 K

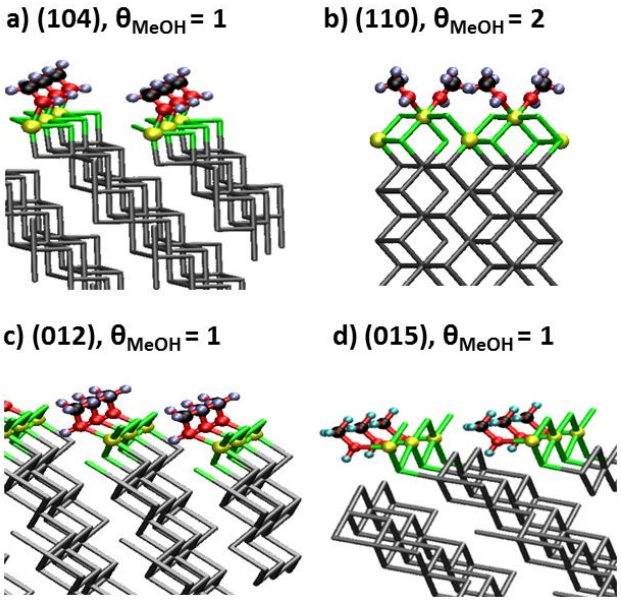


Figure 4. Optimized $MgCl_2$ surfaces in presence of adsorbed methanol. Bulk $MgCl_2$ is represented in grey. Surface chlorine and magnesium atoms are shown in green and yellow, respectively. C, O and H atoms of adsorbed methanol are shown in black, red and white.

the stability of all the surfaces increases with respect to naked $MgCl_2$, but at a different extent. In particular, the surfaces more affected by methanol coordination are the penta-coordinated (012) and (101), which becomes the most stable, and the tetra-coordinated (110), which becomes at a degree of coverage $\theta_{MeOH} = 2$ more stable than the traditional (104). At T = 373 K, adsorption of methanol further stabilizes the (015) surface, so that it competes in stability with the low lying (in energy) (012) and (101) families of penta-coordinated surfaces. In contrast, the (104) and (107) surfaces are highly disfavoured by methanol adsorption ($\Delta G_{ads} > 0$). In conclusion, our calculations of involved $\Delta G_{ads}$ indicate that in presence of methanol at 373 K the $MgCl_2$ nano-crystals should express at the same extent the penta-coordinated (012) and the

(015) families of surfaces, followed by the tetra-coordinated (110) ones.

Representations of the main $MgCl_2$ surfaces in the presence of methanol are reported in Figure 4. The (015) surface shows a unusual flexibility in presence of methanol, in that the Mg cations are displaced from the Cl underneath. The structure of the (015) surface in presence of an adsorbate recalls the nano-ribbons that have been hypothesized to form from bulk $MgCl_2$ upon activation by milling,[49,60] with flat chains of tetra-coordinated Mg sites having the four chlorine ligands bridging in a square planar coordination. The distance between a Mg ion in the "ribbon" and a Cl underneath (deeper layer) is about 0.3 Å larger than the Mg-Cl intra-ribbon distance. This leaves a sort of channel between the upper layer and the layers above. For this reason, the Mg sites at the (015) surface display an asymmetric local environment and, once that methanol is removed, they may bind differently molecules on the upper and down face. This asymmetry could induce the formation of asymmetric Ti sites once that the pre-catalyst is

**Table 2. Predicted adsorption energies ($\Delta E_{ads}$ and $\Delta G_{ads}$) for methanol on different $MgCl_2$ surfaces, and predicted stability (in terms of Gibbs free energy, in J/m$^2$) of each surface in presence of methanol in the gas phase ($G_{s\text{-}MeOH(g)}$) and in the liquid phase ($G_{s\text{-}MeOH(l)}$). Calculations in the gas phase were performed at 298 K and 373 K. All data are corrected by BSSE using the counterpoise method.**

| Surface | $\theta_{MeOH}$ | $\Delta E_{ads}$ (kJ/mol) | $\Delta G_{ads}$ (kJ/mol) | | $G_{s\text{-}MeOH(g)}$ (J/m$^2$) | | $G_{s\text{-}MeOH(l)}$ (J/m$^2$) |
|---|---|---|---|---|---|---|---|
| | | | T = 298K | T= 373K | T = 298K | T= 373K | T = 298K |
| (001) | 1 | -34.9 | +35.4 | | 0.0498 | 0.0429 | 0.0498 |
| (101) | 1 | -112.1 | -41.3 | -28.3 | 0.287 | 0.458 | 0.320 |
| (012) | 1 | -124.5 | -51.1 | -37.5 | 0.183 | 0.337 | 0.215 |
| (104) | 1 | -76.4 | -7.84 | +7.40 | 0.633 | 0.835 | 0.659 |
| (015) | 1 | -87.0 | -20.9 | -9.10 | 0.336 | 0.450 | 0.361 |
| (107) | 1 | -79.3 | -11.1 | +1.11 | 0.334 | 0.447 | 0.354 |
| (110) | 1 | -107.7 | -42.1 | -30.4 | 0.720 | 0.899 | 0.740 |
| (110) | 2 | -100.7 | -32.1 | -19.6 | 0.576 | 0.810 | 0.614 |

constructed, and may eventually influence the catalytic event after catalyst activation. As a final comment, based on X-ray powder diffraction data, Auriemma and De Rosa[48,49] suggested partially folded $[MgCl_2(donor)_n]_x$ chains (rather than linear ones) as intermediate structures on the way from precursor $MgCl_2$ donor adducts to base-free $MgCl_2$. Further calculations on larger cells (with different position for alcohol or 'donor') would provide information on the regular repetition of the ribbon-like structure along the face and would say whether or not this is the case.

**4.3 Surface properties of activated $MgCl_2$.** According to our synthetic procedure, the $MgCl_{2\text{-}act}$ nano-crystals are formed in the presence of methanol at a temperature between 298 and 473 K. In these conditions, if we endorse the conclusions of the previous section, methanol should act as a shape-directing agent, and should strongly favour the formation of small crystals prevalently exposing the (012), (015) and (110) surfaces. When industrial synthesis procedures are employed, the methanol molecules (or other simple alcohol molecules) acting as stabilizers for these surfaces may easily be removed by the reaction with $TiCl_4$. Hence, $TiCl_4$ would find suitable surfaces for chemisorption. Our experimental approach allows to study those surfaces even without the presence of $TiCl_4$. Indeed, once the $MgCl_2$ nano-crystals are shaped in presence of excess of methanol, they experience a prolonged annealing procedure at 473 K in high vacuum. This step slowly removes the adsorbed methanol, leaving the surfaces in a metastable state and hence available for adsorption of probe molecules. As a matter of fact, the FT-IR spectrum of $MgCl_{2\text{-}act}$ at the end of the activation step (Figure S2) does reveal the presence of only minor amount of methanol, indicating that most of the tetra-coordinated and penta-coordinated surfaces display at least one coordination vacancy available for CO adsorption.

On these basis, we decided to investigate the surface properties of $MgCl_{2\text{-}act}$ by means of in situ FT-IR spectroscopy of CO adsorbed at 100 K. This method has been largely employed in the past to obtain a detailed description of the surface properties of a variety of high-surface-area materials,[61-63] although it was rarely applied to investigate metal-halides. In particular, to the best of our knowledge, the only experimental report on CO adsorption on $MgCl_2$ is that of Zakharov et al.,[64] later on interpreted by theoretical calculations performed on small relaxed $MgCl_2$ clusters.[65]

Figure 5 shows the FT-IR spectra of CO adsorbed at 100 K on $MgCl_{2\text{-}act}$ as a function of CO equilibrium pressure (starting from an equilibrium pressure $P_{CO}$ = 50 Torr). Two IR absorption bands are observed in the 2200-2150 cm$^{-1}$ range, whose position is a function of the CO surface coverage ($\theta_{CO}$). The most intense one is located at 2182 cm$^{-1}$ for maximum $\theta_{CO}$, and undergoes a very large shift upon decreasing CO coverage, going to 2194 cm$^{-1}$ for $\theta_{CO} \rightarrow 0$. The second absorption band is much less sensitive to the decrease of $\theta_{CO}$, and shifts from 2159 cm$^{-1}$ at maximum $\theta_{CO}$ to 2163 cm$^{-1}$ for $\theta_{CO} \rightarrow 0$. At the maximum $\theta_{CO}$ the two bands are separated of $\Delta\tilde{\nu}$ = 23 cm$^{-1}$. Both absorption bands are completely reversible upon degassing the cell at 100 K, indicating that the interaction between CO and $MgCl_2$ surfaces is quite weak. Our spectra are similar, but not the same, as that reported by Zakharov et al.[64] In that case a complex envelop of bands with maxima at 2210, 2190 and 2170 cm$^{-1}$ (for CO dosed at room temperature and $P_{CO}$ = 1 atm) was reported, but for CO adsorbed on a $MgCl_2$ obtained by reacting Mg powder with

butyl chloride (and hence possible different from a morphological point of view).

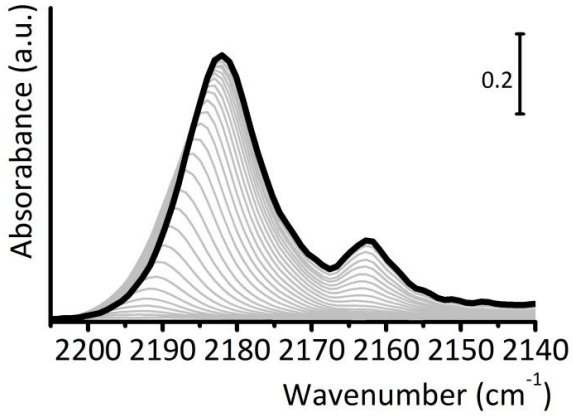


Figure 5. FT-IR spectra (in the $\tilde{\nu}$(CO) region) of CO adsorbed at 100 K on $MgCl_{2\text{-act}}$ as a function of the CO coverage (maximum $\theta_{CO}$ in bold). The spectra are shown after subtraction of the spectrum of $MgCl_{2\text{-act}}$.

**Table 3. Energetic of adsorption for CO molecules adsorbed on the main $MgCl_2$ surfaces, both at 298 K and at 100 K, predicted $\tilde{\nu}$(CO) values and corresponding shift ($\Delta\tilde{\nu}$) with respect to $\tilde{\nu}$(CO) of gaseous phase (2216.8 $cm^{-1}$ and 2189.9 $cm^{-1}$, calculated at TZVP and QZVP levels, respectively), and predicted intensity (arbitrary units).**

| surface | $\Delta E_{ads}$ (kJ/mol) | $\Delta G_{ads}$ (kJ/mol) | $\Delta G_{ads}$ (kJ/mol) | $\tilde{\nu}$ ($cm^{-1}$) | $\tilde{\nu}$ ($cm^{-1}$) | $\Delta\tilde{\nu}$ ($cm^{-1}$) | Intensity (a.u.) |
|---|---|---|---|---|---|---|---|
| | | T=298K | T=100K | TZVP | QZV2P | QZV2P | QZV2P |
| (012) | -44.5 | -2.4 | -26.2 | - | 2268.3 | +78.4 | 164.1 |
| (104) | -32.1 | 2.2 | -18.9 | 2279.1 | 2243.5 | +53.6 | 125.0 |
| (015) | -42.7 | -3.7 | -27.5 | - | 2266.1 | +76.2 | 234.2 |
| (107) | -36.0 | -1.5 | -22.4 | - | 2245.7 | +55.8 | 133.9 |
| (110) | -39.9 | -5.5 | -27.0 | 2275.1 | 2260.8 | +70.9 | 133.9 |

The two absorption bands observed in Figure 5 reveal the formation of mono-carbonyl species characterized by a relevant polarization on two different types of $Mg^{2+}$ sites. The IR absorption band at lower wavenumber values is tentatively assigned to CO adsorbed on penta-coordinated $Mg^{2+}$ sites ($Mg_{5c}^{2+}$), whereas the second band is assigned to CO adsorbed on tetra-coordinated $Mg^{2+}$ sites ($Mg_{4c}^{2+}$). As a matter of fact, being less coordinated, a $Mg_{4c}^{2+}$ site is more polarizing than a $Mg_{5c}^{2+}$ site. To exclude the possible presence of di-carbonyl species, which are virtually possible on $Mg_{4c}^{2+}$ sites, the same experiment was repeated in the presence of an isotopic mixture of $^{12}CO$-$^{13}CO$, as shown in Figure S4. The FT-IR spectra collected in the presence of the isotopic mixture are a replica of those obtained in presence of $^{12}CO$ only, but shifted of the expected isotopic ratio. No additional IR absorption bands are observed at intermediate $\tilde{\nu}$(CO) values, as expected for mixed di-carbonyl species. Hence, despite the availability of two potential coordination vacancies on surfaces exposing $Mg_{4c}^{2+}$ sites, only one CO molecule is adsorbed in our experimental conditions. Finally, it is worth noticing that defects sites (such as steps and corners) likely present at the surface of $MgCl_{2\text{-act}}$ nano-crystals and recently proposed as possible sites for strong $TiCl_4$ adsorption,[66,67] were not detected essentially because they are still covered by methanol residues.

The aforementioned assignment, based on common sense, is supported by our DFT-D theoretical calculations, although a few unexpected results have been obtained. Table 3 reports the predicted energetic of adsorption for CO molecules ($\Delta G_{ads}$) on different $MgCl_2$ surfaces at full coverage ($\theta_{CO}$ = 1) at both room temperature and 100 K, the predicted $\tilde{\nu}$(CO) and the $\Delta\tilde{\nu}$ values with respect to free CO molecule, and the predicted intensity. In agreement with the experimental observation, the CO adsorption energy is weak on all the surfaces also at 100 K, and the interaction is stronger with the tetra-coordinated surfaces. Calculated $\Delta\tilde{\nu}$ values are slightly overestimated with respect to the experimentally observed ones, as expected because the adopted basis set does not reproduce correctly the properties of the molecule in the gas phase. However, CO adsorbed on the penta-coordinated (104) and (107) surfaces is characterized by the lowest $\tilde{\nu}$(CO) value (in average 2244 $cm^{-1}$), about 22 – 17 $cm^{-1}$ lower than the $\tilde{\nu}$(CO) for CO adsorbed on the (110) surface. These values are in very good agreement with the experimental value of 23 $cm^{-1}$ that separates the two absorption bands assigned to penta- and tetra-coordinated surfaces, respectively. Surprisingly, the calculated $\tilde{\nu}$(CO) for CO adsorbed on the penta-coordinated (012) and (015) surfaces is almost equivalent to that of CO adsorbed on the tetra-coordinated surface, despite a lower polarizing ability is expected for a penta-coordinated $Mg^{2+}$ cation. We explain this $\tilde{\nu}$(CO) value by considering that a CO molecule adsorbed at the (012) and (015) surfaces is influenced by the chlorine ligands belonging to neighbouring layer, very close to the oxygen of the adsorbed CO molecule.

Due to the negligible difference between the predicted $\tilde{\nu}$(CO) for CO adsorbed on the (110), (015) and (012) surfaces, we can reasonable assume that the highest wavenumber band

observed in the spectra shown in Figure 5 can be interpreted in terms of a superposition of the three contributions. A short comment should be done on the relative intensities of the two absorption bands. Although the computed intensities depending on Born charge estimates are not highly accurate, the relative intensity for CO adsorbed on the (015) surface is about 1.9 and 1.7 higher than those of CO adsorbed on the (012) and (110) surfaces, respectively. This indicates that the (015) surface is the most observable by CO adsorption. By considering the estimated extinction coefficients, the spectra shown in Figure 5 suggest an almost equal amount of tetra- and penta-coordinated surfaces, in well agreement with the morphological predictions discussed in the previous section.

Finally, the behaviour of the two experimentally observed $\tilde{\nu}$(CO) absorption bands as a function of $\theta_{CO}$ merits a comment. As largely documented in the specialized literature for other metal chlorides and for a large number of metal oxides,[61] the blue shift of both absorption bands observed upon decreasing $\theta_{CO}$ is a clear evidence that the adsorbing cationic sites belong to extended and regular surfaces. In these conditions, at high $\theta_{CO}$, the adsorbed CO molecules behave as coupled oscillators and consequently, $\tilde{\nu}$(CO) is shifted at lower wavenumber values. The coupling gradually vanishes with lowering the coverage, with a consequent increase of the $\tilde{\nu}$(CO) value. The shift is larger for CO adsorbed on the (015), (110) and (012) surfaces, indicating that on these sites the adsorbed OC molecules can easily couple to each other at the highest coverage.

**4.4 Surface properties of $MgCl_{2\text{-}act}/TiCl_4$ pre-catalyst.** In a successive step, $MgCl_{2\text{-}act}$ sample was titanated to obtain the $MgCl_{2\text{-}act}/TiCl_4$ pre-catalyst. The titanation procedure, described in the experimental section, resulted in a titanium concentration of about 1 wt%, which is comparable to the titanium loading in industrial pre-catalysts. The so obtained pre-catalysts did show the same XRPD patterns of the corresponding $MgCl_{2\text{-}act}$ supports. In order to investigate where $TiCl_4$ is bonded on $MgCl_2$, we collected FT-IR spectra of CO adsorbed at 100 K on the pre-catalyst, following the same procedure as for $MgCl_{2\text{-}act}$. Figure 6 shows the FT-IR spectra of CO adsorbed at 100 K on the $MgCl_{2\text{-}act}/TiCl_4$ pre-catalyst as a function of $\theta_{CO}$, compared to the spectrum of CO adsorbed on $MgCl_{2\text{-}act}$ at the maximum $\theta_{CO}$. After reaction with $TiCl_4$, the IR absorption band assigned to CO adsorbed on the $Mg_{4c}^{2+}$ sites and/or on the (012) surface greatly decreases in intensity (although it does not disappear completely), whereas the band assigned to CO adsorbed on the $Mg_{5c}^{2+}$ sites belonging to the (104) and (107) surfaces is almost unaffected (i.e. these surfaces are still available for CO adsorption). These data suggest that $TiCl_4$ preferentially binds to the (110) surface, in perfect agreement with recent theoretical calculations[14] and with previous experimental data,[68,69] but also on the (015) and (012) surfaces. However, the adsorption energy for $TiCl_4$ on the (012) surface was estimated to be -41.4 kJ/mol at the B3LYPD-2D level (and -61.1 kJ/mol at M06 single point), which is by far too low for stable adsorption under conditions representative of catalyst preparation.[41] Hence, we have to conclude that the weak absorption band still observable around 2182 $cm^{-1}$ (for maximum $\theta_{CO}$) in the spectra of CO adsorbed on the $MgCl_{2\text{-}act}/TiCl_4$ pre-catalyst is due to CO adsorbed on the (012) surface.

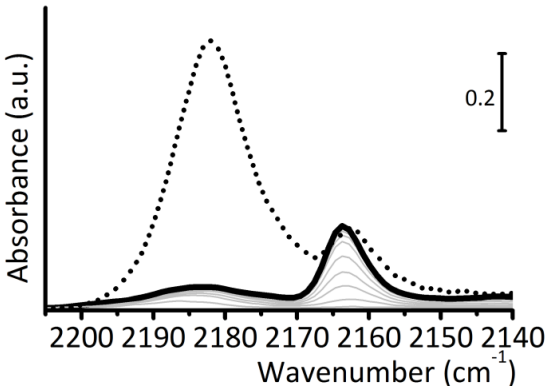


Figure 6. FT-IR spectra (in the $\tilde{\nu}$(CO) region) of CO adsorbed at 100 K on $MgCl_{2\text{-}act}/TiCl_4$ pre-catalyst as a function of the CO coverage (maximum $\theta_{CO}$ in bold). The spectra are shown after subtraction of the spectrum of $MgCl_{2\text{-}act}$. Also the spectrum of CO adsorbed on $MgCl_{2\text{-}act}$ at the maximum $\theta_{CO}$ is shown for comparison (dotted).

## 5. CONCLUSIONS

Structurally disordered activated $MgCl_2$ nano-crystals were synthetized through a controlled de-alcoholation of the $MgCl_2 \cdot 6MeOH$ precursor and extensively characterized in terms of structure, morphology and surface properties. Our synthetic method, which mimics that routinely adopted to prepare industrial Ziegler-Natta catalysts,[29,30] allowed obtaining well-defined crystals of nanometric dimensions as observed by HR-TEM, with a surface area as high as 100 $m^2/g$, a value comparable with that characteristic of industrially relevant $MgCl_2$ prepared by chemical or mechanical methods.[53,54] Successively, the $MgCl_{2\text{-}act}$ nano-crystals shaped in presence of methanol at a temperature between 300 K and 473 K, were subjected to a prolonged degassing step at 473 K, which lead to an almost complete removal of the adsorbed methanol. This procedure left the exposed surfaces in a metastable state and hence available for adsorption of probe molecules. FT-IR spectroscopy of CO adsorbed at 100 K was adopted to probe the exposed surfaces. The experimental data were compared with DFT-D computational results, obtained by a systematic investigation of the stability of the $MgCl_2$ surfaces in presence of methanol, for the first time considering the entropic contribution. The main results obtained by our tandem approach are as follows.

1) A never mentioned surface has been discovered (the (015) one) that, in the naked crystal, is locally similar to the traditional penta-coordinated ones, but is characterized by distorted Cl-Mg-Cl angles. This surface displays an unusual flexibility in the presence of adsorbates, which detach the Mg cations from the Cl underneath, leaving a coordination vacancy available for the binding of asymmetric titanium sites. The (015) surface, as well as the tetra-coordinated (110) one, are highly stabilized by methanol adsorption (in agreement with previous works)[11-13] especially when higher temperature, typical of catalysts preparation in industry, are considered. Hence, both of them are expected to contribute to the morphology of the $MgCl_2$ nano-crystals obtained from alcohol adducts.
2) Our calculation clearly show that the penta-coordinated surfaces do not behave in the same way in presence of

methanol as adsorbate, being the (012) and (101) highly stabilized, and the (104) and (107) disfavoured. Hence, the first family of surfaces shall be expressed in the $MgCl_2$ nano-crystals formed in presence of methanol in a much larger extent than the second one.

3) FT-IR spectroscopy of adsorbed CO revealed to be a powerful method to experimentally probe the exposed $MgCl_2$ surfaces and determine the relative proportion of the penta-coordinated and tetra-coordinated ones. DFT-D calculations correctly predicted the energy of CO adsorption and well reproduced the experimental $\tilde{\nu}$(CO) values for CO adsorbed on both tetra- and penta-coordinated $MgCl_2$ surfaces.
4) The same technique provides also a clear experimental evidence that $TiCl_4$ binds to tetra-coordinated surfaces, in agreement with previous theoretical[14] and experimental[68,69] findings.
5) Although HR-TEM pictures and XRD measurements demonstrate that $MgCl_{2\text{-act}}$ is in the form of crystals of nano-metric dimension with only a very low number of regularly stacked layers, CO molecules probe locally regular surfaces. This indicates that the computational approach adopted in this work is valuable to model $MgCl_2$ nano-crystals, either obtained by harsh ball-milling or assembled after de-alcoholation process. Obviously, the presence of defective sites cannot be excluded; if present these sites are likely blocked by residual alcohol molecules and hence not accessible by CO.

The novelty of this work relies in the synergic combination of an innovative experimental approach (based on a step-by-step controlled synthesis and advanced characterization) with a systematic computational modelling which takes into account also the usually neglected entropic contribution at harmonic vibrational level. On one side, FT-IR spectroscopy of CO adsorbed at 100 K emerges as a feasible, simple and powerful method to characterize the surface of structurally disordered $MgCl_2$-based Ziegler-Natta catalysts, provided that all the synthetic steps are carefully conducted. This methods has the advantage to overcome the fluorescence problems of Raman spectroscopy in presence of organic residues, thus opening new perspectives in the characterization of Ziegler-Natta catalysts. On the other side, our computational morphological analysis reveals the presence of two, non-equivalent, tetra-coordinated surfaces which are highly stabilized by methanol as an electron donor, especially at the temperature typically adopted in the preparation of the pre-catalysts. Since the recent literature identified a tetra-coordinated Mg as a site of election for the deposition of the Ti species relevant in olefin polymerization,[41] independently on the role of each component in the catalytic mixture and before considering any mechanistic prediction, the presence of two eligible Mg sites for Ziegler-Natta catalysis seems to us of high interest and might reconcile the traditional vision on Ziegler-Natta catalysis with the recent experimental and theoretical results. In fact, we expect that the relative occurrence of each site, depending on the preparation conditions (in particular the alcohol employed in the preparation, the presence or not of other donors, the temperature control), may influence the distribution of the reduced Ti sites and in turn the weight distribution and consequently the catalytic performances and the technological properties of the final polymer product.

## ASSOCIATED CONTENT

**Supporting Information.** TGA profile for the $MgCl_2 \cdot 6MeOH$ precursor; FT-IR spectrum og $MgCl_{2\text{-act}}$; FT-IR spectra of a 1:1 isotopic mixture of $^{12}CO$-$^{13}CO$ adsorbed at 100 K on $MgCl_{2\text{-act}}$ as a function of $\theta_{CO}$. This material is available free of charge via the Internet at http://pubs.acs.org.

## AUTHOR INFORMATION

### Corresponding Author

* E-mail: elena.groppo@unito.it

### Author Contributions

All authors have given approval to the final version of the manuscript.

### Funding Sources

This work has been supported by the Progetto di Ateneo/CSP 2014 (Torino_call2014_L1_73).

## ACKNOWLEDGMENT

Federica Franconieri is kindly acknowledged for the HR-TEM images. We are grateful to Adriano Zecchina, Gabriele Ricchiardi, Bartolomeo Civalleri and Piero Ugliengo for the useful discussion. The computational work was performed on the Abel Cluster, owned by the University of Oslo and the Norwegian metacenter for High Performance Computing (NOTUR), and operated by the Department for Research Computing at USIT, the University of Oslo IT-department. http://www.hpc.uio.no/.

## REFERENCES

(1) Busico, V., *MRS Bulletin* **2013**, *38*, 224-228.
(2) Albizzati, E.; Giannini, U.; Collina, G.; Noristi, L.; Resconi, L., *Catalysts and polymerizations*, in: Polypropylene Handbook; Moore, E. P. J., Ed.; Hanser-Gardner Publications: Cincinnati, OH, **1996**.
(3) Karol, F. J., *Catal. Rev. Sci. Eng.* **1984**, *26*, 557.
(4) Karol, F. J.; Cann, K. J.; Wagner, B. E., in: Transition Metals and Organometallics as Catalysts for Olefin Polymerization; Kaminsky, W.; Sinn, H., Ed.; Springer: Berlin, Germany, **1988**, p. 149.
(5) Kissin, Y. V., in: Alkene Polymerization Reactions with Transition Metal Catalysts; Elsevier: Amsterdam, The Netherlands, **2008**.
(6) Nowlin, T. E.; Mink, R. I.; Kissin, Y. V., in: Transition Metal Polymerization Catalysts; Hoff, R.; Mathers, R. T., Ed.; John Wiley & Sons: Hoboken, USA., **2009**.
(7) Nowlin, T. E., *Business and Technology of the Global Polyethylene Industry*, in; Scrivener Publishing LLC: New York, **2014**.
(8) Corradini, P.; Barone, V.; Fusco, R.; Guerra, G., *Gazz. Chim. Ital.* **1983**, *113*, 601.
(9) Corradini, P.; Guerra, G.; Cavallo, L., *Acc. Chem. Res.* **2004**, *37*, 231-241.
(10) Busico, V.; Causa, M.; Cipullo, R.; Credendino, R.; Cutillo, F.; Friederichs, N.; Lamanna, R.; Segre, A.; Castellit, V. V., *J. Phys. Chem. C* **2008**, *112*, 1081-1089.
(11) Capone, F.; Rongo, L.; D'Amore, M.; Budzelaar, P. H. M.; Busico, V., *J. Phys. Chem. C* **2013**, *117*, 24345-24353.
(12) Credendino, R.; Pater, J. T. M.; Correa, A.; Morini, G.; Cavallo, L., *J. Phys. Chem. C* **2011**, *115*, 13322-13328.
(13) Turunen, A.; Linnolahti, M.; Karttunen, V. A.; Pakkanen, T. A.; Denifl, P.; Leinonen, T., *J. Mol. Catal. A Chem.* **2011**, *334*, 103-107.
(14) D'Amore, M.; Credendino, R.; Budzelaar, P. H. M.; Causá, M.; Busico, V., *J. Catal.* **2012**, *286*, 103-110.
(15) Groppo, E.; Seenivasan, K.; Barzan, C., *Catal. Sci. Technol.* **2013**, *3*, 858-878.
(16) Magni, E.; Somorjai, G. A., *Catal. Lett.* **1995**, *35*, 205-214.

(17) Magni, E.; Somorjai, G. A., *App. Surf. Sci.* **1995**, *89*, 187-195.
(18) Magni, E.; Somorjai, G. A., *Surf. Sci.* **1995**, *341*, L1078-L1084.
(19) Magni, E.; Somorjai, G. A., *J. Phys. Chem.* **1996**, *100*, 14786-14793.
(20) Magni, E.; Somorjai, G. A., *Surf. Sci.* **1997**, *377*, 824-827.
(21) Magni, E.; Somorjai, G. A., *J. Phys. Chem. B* **1998**, *102*, 8788-8795.
(22) Schmidt, J.; Risse, T.; Hamann, H.; Freund, H. J., *J. Chem. Phys.* **2002**, *116*, 10861-10868.
(23) Risse, T.; Schmidt, J.; Hamann, H.; Freund, H. J., *Angew. Chem.-Int. Edit.* **2002**, *41*, 1518-1520.
(24) Freund, H. J.; Baumer, M.; Libuda, J.; Risse, T.; Rupprechter, G.; Shaikhutdinov, S., *J. Catal.* **2003**, *216*, 223-235.
(25) Andoni, A.; Chadwick, J. C.; Niemantsverdriet, H. J. W.; Thune, P. C., *Macromol. Rapid Commun.* **2007**, *28*, 1466-1471.
(26) Andoni, A.; Chadwick, J. C.; Milani, S.; Niemantsverdriet, H.; Thune, P. C., *J. Catal.* **2007**, *247*, 129-136.
(27) Andoni, A.; Chadwick, J. C.; Niemantsverdriet, H. J. W.; Thune, P. C., *J. Catal.* **2008**, *257*, 81-86.
(28) Andoni, A.; Chadwick, J. C.; Niemantsverdriet, J. W.; Thune, P. C., *Catal. Lett.* **2009**, *130*, 278-285.
(29) Giannini, U.; Albizzati, E.; Parodi, S.; Pirinoli, F., Catalysts for polymerizing olefins. US Patent 4,124,532, November 7, 1978.
(30) Evangelisti, D.; Collina, G.; Fusco, O.; Sacchetti, M., Magnesium dichloride-ethanol adduct and catalyst components obained therefrom. US 7,087,688 B2, 2006.
(31) Wulff, G., *Zeitsch. für Kristall.* **1901**, *34*, 449–480.
(32) Gibbs, J. W., *The collected works*; Longmans: New-York, **1928**.
(33) Gnanakumar, E. S.; Gowda, R. R.; Kunjir, S.; Ajithkumar, T. G.; Rajamohanan, P. R.; Chakraborty, D.; Gopinath, C. S., *ACS Catal.* **2013**, *3*, 303-311.
(34) Thushara, K. S.; Gnanakumar, E. S.; Mathew, R.; Jha, R. K.; Ajithkumar, T. G.; Rajamohanan, P. R.; Sarma, K.; Padmanabhan, S.; Bhaduri, S.; Gopinath, C. S., *J.Phys.Chem.C* **2011**, *115*, 1952-1960.
(35) CRYSTAL14 User's Manual. Dovesi, R.; Orlando, R.; Erba, A.; Zicovich-Wilson, C. M.; Civalleri, B.; Casassa, S.; Maschio L.; Ferrabone, M.; De La Pierre, M.; D'Arco, P.; Noel, Y.; Causa, M.; Rerat, M.; B. Kirtman. B.; *Int. J. Quantum Chem.* **2014**, *114*, 1287-1292.
(36) Becke, A. D., *J. Chem. Phys.* **1993**, *98*, 5648-5652.
(37) Grimme, S. J., *Comput. Chem.* **2006**, *27*, 1787-1799.
(38) Civalleri, B.; Zicovich-Wilson, C. M.; Valenzano, L.; Ugliengo, P., *CrystEngComm* **2008**, *10*, 405−410.
(39) Schäfer, A.; Horn, H.; Ahlrichs, R., *J. Chem. Phys.* **1992**.
(40) Prencipe, M.; Pascale, F.; Zicovich-Wilson, C. M.; Saunders, V. R.; Orlando, R.; Dovesi, R., *Phys. Chem. Miner.* **2004**, *31*, 1−6.
(41) D'Amore, M.; Credendino, R.; Budzelaar, P. H. M.; Causa, M.; Busico, V., *J. Catal.* **2012**, *286*, 103-110.
(42) Pascale, F.; Zicovich-Wilson, C. M.; Gejo, F. L.; Civalleri, B.; Orlando, R.; Dovesi, R., *J. Comput. Chem.* **2004**, *25*, 888-897.
(43) Zicovich-Wilson, C. M.; Pascale, F.; Roetti, C.; Saunders, V. R.; Orlando, R.; Dovesi, R., *J. Comput. Chem.* **2004**, *25*, 1873-1881.
(44) Pascale, F.; Zicovich-Wilson, C. M.; Orlando, R.; Roetti, C.; Ugliengo, P.; Dovesi, R., *J. Phys. Chem. B* **2005**, *109*, 6146-6152.
(45) For further details see tutorial: Extracting nanorods and nanocrystals, at http://www.crystal.unito.it/.
(46) Civalleri, B.; Maschio, L.; Ugliengo, P.; Zicovich-Wilson, C. M., *Phys.Chem.Chem.Phys.* **2010**, *12*, 6382-6386.
(47) Dall'Olio, S.; Dovesi, R.; Resta, R., *Phys. Rev. B* **1997**, *56*, 10105-10114.
(48) Auriemma, F.; De Rosa, C., *Chem. Mater.* **2007**, *19*, 5803-5805.
(49) Auriemma, F.; De Rosa, C., *J. Appl. Crystallog.* **2008**, *41*, 68-82.
(50) Huang, R.; Malizia, F.; Pennini, G.; Koning, C. E.; Chadwick, J. C., *Macromol. Rapid Commun.* **2008**, *29*, 1732-1738.
(51) Malizia, F.; Fait, A.; Cruciani, G., *Chem. Eur. J.* **2011**, *17*, 13892-13897.
(52) Chang, M.; Liu, X.; Nelson, P. J.; Munzing, G. R.; Gegan, T. A.; Kissin, Y. V., *J. Catal.* **2006**, *239*, 347–353.
(53) Gerbasi, R.; Marigo, A.; Martorana, A.; Zannetti, R.; Guidetti, G. P.; Baruzzi, G., *Eur Polym J* **1984**, *20*, 967-970.
(54) JalaliDil, E.; Pourmahdian, S.; Vatankhah, M.; Taromi, F. A., *Polym. Bull.* **2010**, *64*, 445-457.
(55) McKenna, T. F. L.; Di Martino, A.; Weickert, G.; Soares, J. B. P., *Macromol. React. Eng.* **2010**, *4*, 40-64.
(56) Oleshko, V. P.; Crozier, P. A.; Cantrell, R. D.; Westwood, A. D., *Macromol. Rapid Commun.* **2001**, *22*, 34-40.
(57) Mori, H.; Sawada, M.; Higuchi, T.; Hasebe, K.; Otsuka, N.; Terano, M., *Macromol. Rapid Commun.* **1999**, *20*, 245-250.
(58) Credendino, R.; Busico, V.; Causa, M.; Barone, V.; Budzelaar, P. H. M.; Zicovich-Wilson, C., *Phys. Chem. Chem. Phys.* **2009**, *11*, 6525-6532.
(59) Note that normal modes with frequencies below 100 $cm^{-1}$ are present in the vibrational spectrum of every slab, slightly more abundant for the (110) surface. This could justify why the vibrational correction for the (110) surface is almost twice the average correction for the other surfaces. Correcting for anharmonicity could give more accurate results, but it is out of the capability for periodic calculation with large models like those investigated.
(60) Vittadello, M.; Stallworth, P. E.; Alamgir, F. M.; Suarez, S.; Abbrent, S.; Drain, C. M.; Di Noto, V.; Greenbaum, S. G., *Inorg. Chim. Acta* **2006**, *359*, 2513-2518.
(61) Zecchina, A.; Scarano, D.; Bordiga, S.; Spoto, G.; Lamberti, C., *Adv. Catal.* **2001**, *46*, 265-397 and references therein.
(62) Lamberti, C.; Groppo, E.; Spoto, G.; Bordiga, S.; Zecchina, A., *Adv. Catal.* **2007**, *51*, 1-74.
(63) Lamberti, C.; Zecchina, A.; Groppo, E.; Bordiga, S., *Chem. Soc. Rev.* **2010**, *39*, 4951–5001.
(64) Zakharov, V. A.; Paukshtis, E. A.; Mikenas, T. B.; Volodin, A. M.; Vitus, E. N.; Potapov, A. G., *Macromol. Symp.* **1995**, *89*, 55.
(65) Trubitsyn, D. A.; Zakharov, V. A.; Zakharov, I. I., *J. Mol. Catal. A-Chem.* **2007**, *270*, 164-170.
(66) Credendino, R.; Liguori, D.; Fan, Z.; Morini, G.; Cavallo, L., *ACS Catal.* **2015**, *5*, 5431-5435.
(67) Correa, A.; Bahri-Laleh, N.; Cavallo, L., *Macromol. Chem. Phys.* **2013**, *214*, 1980-1989.
(68) Brambilla, L.; Zerbi, G.; Nascetti, S.; Piemontesi, F.; Morini, G., *Macromol. Symp.* **2004**, *213*, 287-301.
(69) Brambilla, L.; Zerbi, G.; Piemontesi, F.; Nascetti, S.; Morini, G., *J. Mol. Catal. A-Chem.* **2007**, *263*, 103-111.